

# Text-Guided Visual Representation Learning for Robust Multimodal E-Commerce Recommendation

Yufei Guo  
guoyufei21@mails.tsinghua.edu.cn  
Tsinghua University  
Beijing, China

Shijie Yang  
yangshijie30@jd.com  
JD.COM  
Beijing, China

Jing Ma  
ma-j22@mails.tsinghua.edu.cn  
Tsinghua University  
Beijing, China

Yanlong Zang  
zangyanlong1@jd.com  
JD.COM  
Beijing, China

Tianlu Zhang  
tlzhang@mail.tsinghua.edu.cn  
Tsinghua University  
Beijing, China

Weijie Ding  
dingweijie8@jd.com  
JD.COM  
Beijing, China

Pinghua Gong  
gongpinghua1@jd.com  
JD.COM  
Beijing, China

Jungong Han  
jghan@mail.tsinghua.edu.cn  
Tsinghua University  
Beijing, China

## Abstract

Multimodal item embeddings are crucial for e-commerce item-to-item (I2I) retrieval, yet real-world product images often contain promotional overlays and background clutter that inject spurious visual cues and degrade retrieval robustness. This issue is particularly pronounced in MLRM-style pipelines, where a frozen vision encoder is connected to an LLM through a lightweight connector that must selectively aggregate visual tokens. We propose Text-Guided Q-Former (TGQ-Former), a text-guided visual representation learning framework that leverages structured metadata as semantic guidance for visual token extraction while preserving complementary visual evidence. Concretely, TGQ-Former employs a hybrid-query connector to disentangle metadata-anchored and exploratory visual streams, and introduces a lightweight reliability-aware dual-gated vector modulation module to adaptively calibrate their contributions under noisy inputs. Experiments on large-scale, real-world e-commerce datasets with full-pool retrieval show that TGQ-Former consistently outperforms strong connector baselines and end-to-end MLLMs. On average, it improves Hit Rate@100 (H@100) by 6.04%, demonstrating the effectiveness of text-guided visual encoding for robust multimodal retrieval.

## CCS Concepts

• Information systems → Recommender systems.

## Keywords

E-commerce Recommendation; Large Language Model; Representation Learning; Hybrid-Query Connector

Permission to make digital or hard copies of all or part of this work for personal or classroom use is granted without fee provided that copies are not made or distributed for profit or commercial advantage and that copies bear this notice and the full citation on the first page. Copyrights for components of this work owned by others than the author(s) must be honored. Abstracting with credit is permitted. To copy otherwise, or republish, to post on servers or to redistribute to lists, requires prior specific permission and/or a fee. Request permissions from [permissions@acm.org](mailto:permissions@acm.org).

Conference acronym 'XX, Woodstock, NY

© 2018 Copyright held by the owner/author(s). Publication rights licensed to ACM.

ACM ISBN 978-1-4503-XXXX-X/2018/06

<https://doi.org/XXXXXXXX.XXXXXXX>

## ACM Reference Format:

Yufei Guo, Jing Ma, Tianlu Zhang, Shijie Yang, Yanlong Zang, Weijie Ding, Pinghua Gong, and Jungong Han. 2018. Text-Guided Visual Representation Learning for Robust Multimodal E-Commerce Recommendation. In *Proceedings of Make sure to enter the correct conference title from your rights confirmation email (Conference acronym 'XX)*. ACM, New York, NY, USA, 12 pages. <https://doi.org/XXXXXXXX.XXXXXXX>

## 1 Introduction

Item-to-item (I2I) retrieval is a core component of large-scale e-commerce recommendation systems. It typically operates as a high-recall candidate generation stage, which requires learning retrieval-oriented and discriminative item embeddings under strict latency and throughput constraints [6]. In modern product catalogs, items are typically associated with both visual and structured textual metadata (e.g., title, brand, and hierarchical categories): text offers structured semantic signals, while images capture fine-grained visual attributes. In light of this, the core objective of our work is to learn high-quality multimodal item embeddings, which enable retrieval performance that surpasses single-modality models [4, 26].

In real-world e-commerce, the text modality encompasses product titles and manually curated hierarchical titles at all levels, which can deliver precise semantic information about products. By contrast, product images uploaded by merchants are rarely clean, object-centric photographs. Many of them come from *poster-style listings*, where the product is overlaid with various promotional elements (e.g., sale text, price tags, coupons) and decorative layouts. These non-product visual signals can have mixed effects on item representation: certain contextual presentation details (e.g., standard product packaging, co-displayed matching accessories) can help distinguish visually similar items and even convey their potential application scenarios; in contrast, promotional overlays introduce systematic, marketing-driven visual artifacts that merely correlate with campaign strategies rather than the intrinsic similarity of the products themselves.

Recent advances in LLMs and MLLMs have motivated their adoption in e-commerce recommendation [11, 27, 28]. One common

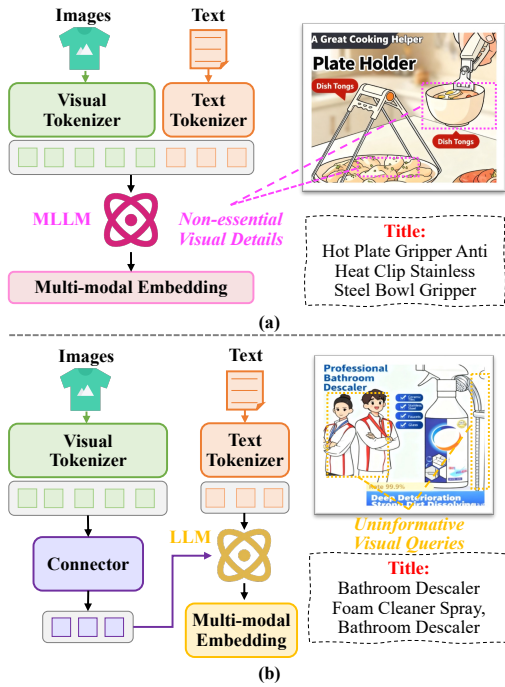


**Figure 1: Illustration of different strategies for using LLMs to enhance multimodal representations. (a) MLLMs based methods. (b) MLRMs based methods.**

paradigm is to directly use an MLLM to map images and text into a unified embedding (Fig. 1(a)), but it is often inefficient for industrial item-to-item (I2I) retrieval. Moreover, MLLMs are typically optimized for generic visual understanding, and their generated representations tend to encode spurious artifacts in e-commerce imagery (e.g., promotional overlays and decorative layouts) that have only weak correlations with intrinsic item similarity. Alternatively, *Multimodal Large Representation Models (MLRMs)* connect a frozen vision encoder to an LLM via a lightweight connector (Fig. 1(b)) [34], offering improved modularity and deployment flexibility. However, existing MLRM approaches overlook the aforementioned image quality issues in e-commerce imagery, which consequently causes their connectors to aggregate visual tokens using learnable queries or naive cross-attention that lack domain-specific semantic grounding. Attention is thus prone to being dominated by visually salient yet product-irrelevant regions, ultimately yielding unstable or distorted item representations in poster-style product listings.

Moreover, we find that simple, training-free preprocessing heuristics (e.g., center cropping) offer only marginal improvements in the presence of promotional overlays (Appendix C). This observation indicates that indiscriminate suppression of non-product regions is impractical in real-world scenarios: valuable contextual cues often coexist with detrimental overlay artifacts, making blind exclusion of non-product content counterproductive. To robustly leverage images in poster-style listings and meet the demands of industrial e-commerce I2I retrieval, a selective approach to utilizing visual evidence is required, rather than a one-size-fits-all multimodal fusion strategy. On one hand, structured metadata (e.g., hierarchical categories and brand) serves as a stable semantic anchor, enabling

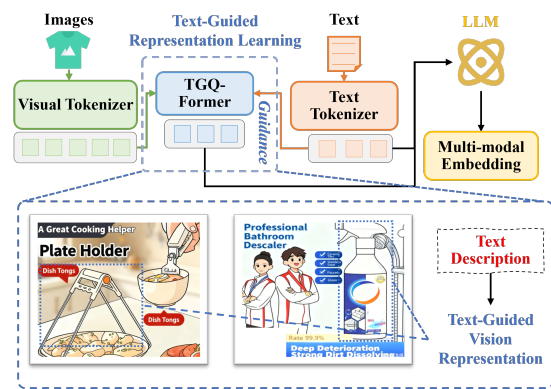


**Figure 2: Illustration of our proposed text-guided visual representation learning paradigm.**

the model to prioritize product-relevant visual cues and alleviate the adverse impact of overlay artifacts. On the other hand, product images inherently contain complementary visual signals that are not fully specified by text and exhibit item-wise variability, including fine-grained appearance details and useful presentation context in real e-commerce listings. These observations motivate a text-guided visual representation learning framework, referred to as **Text-Guided Q-Former (TGQ-Former)**, that uses metadata to steer visual extraction while retaining exploratory learnable queries to capture complementary evidence beyond explicit text.

Specifically, we first propose the **Hybrid-Query Connector**, a connector integrated with a hybrid query set that balances the trade-off between *metadata-anchored* and *exploratory* visual extraction. Metadata-anchored semantic queries leverage structured metadata as a semantic prior to focus on product-relevant visual regions, while exploratory metadata-agnostic learnable queries capture complementary visual signals that lie beyond the scope of explicit textual metadata. Second, we propose the **Dual-Gated Vector Modulation**, a lightweight feature modulation mechanism that adaptively calibrates the two query streams prior to their input into the LLM. Specifically, we modulate the gating of the metadata-anchored query stream according to an image-metadata semantic agreement signal, and regulate the gating of the exploratory query stream based on an item-specific visual reliability signal. Finally, we design the **Redundancy-Reduction Regularizer** to enforce the two query streams to be mutually complementary, and optimize a contrastive retrieval objective by leveraging item embeddings generated by the LLM.

Our contributions are summarized as follows:

- We identify and characterize *poster-style listings* in real-world e-commerce imagery as a systematic source of spurious visual artifacts, where representation learning can drift toward promotional overlay patterns rather than product identity, degrading fine-grained I2I retrieval.

- We propose **TGQ-Former**, a text-guided visual representation learning framework for I2I retrieval. At its core, TGQ-Former introduces a **Hybrid-Query Connector** that disentangles visual evidence into two query streams—metadata-anchored semantic queries and exploratory learnable queries—enabling selective extraction of product-relevant and complementary cues with structured metadata.
- We introduce **Dual-Gated Vector Modulation** together with a **Redundancy-Reduction Regularizer** to perform reliability-aware calibration and complementarity enforcement between the two streams, improving robustness under poster-style and otherwise noisy listings.

## 2 Related Work

### 2.1 Vision–Language Pretraining

Large-scale vision–language pretraining has become a dominant paradigm for multimodal representation learning. Early works such as UNITER [5], OSCAR [19], and ALIGN [14] demonstrated that aligning image and text embeddings enables strong transfer to downstream tasks. Contrastive methods like CLIP [23] and Florence [33] further scale this paradigm to web-scale datasets, achieving remarkable zero-shot generalization. More recent models such as BLIP [15] and BLIP-2 [18] integrate generative and contrastive objectives, and leverage a Query Transformer (Q-Former) to bridge frozen image encoders with LLM backbones. While highly effective for open-domain vision–language tasks, these models are typically trained on data distributions that differ from real-world e-commerce imagery, where promotional overlay artifacts and clutter are prevalent. Our work builds on this line by adapting query-based connectors to retrieval-oriented I2I recommendation, with an emphasis on reliability-aware visual evidence extraction in poster-style listings.

### 2.2 Query-Based Architectures and Robust Cross-Modal Extraction

Query-based architectures have shown promise for efficient cross-modal token extraction. Perceiver [13] and Perceiver-IO [12] demonstrated that a fixed set of latent queries can aggregate information from high-dimensional inputs. Similarly, BLIP-2’s Q-Former [18] uses trainable queries to extract visual features aligned with language backbones. In noisy e-commerce settings, however, relying on a single, semantically unstructured query set can cause cross-attention to be dominated by visually salient yet product-irrelevant regions (e.g., promotional overlay artifacts and decorative layouts), yielding biased representations. Prior work in vision–language grounding and robust representation learning suggests that incorporating semantic priors and confidence/quality signals can improve robustness by steering attention toward task-relevant evidence under diverse input conditions (e.g., grounding with textual/category cues or object-centric priors) [9, 35]. In contrast to methods that inject only a single form of prior, our approach disentangles *anchored semantic evidence* and *exploratory visual evidence* with a hybrid query set, and further performs reliability-aware calibration to prevent overlay artifacts in poster-style listings from dominating retrieval representations.

### 2.3 Item-to-Item Recommendation

Item-to-item (I2I) recommendation is a fundamental component of large-scale recommender systems, often instantiated as a high-recall candidate generation stage prior to ranking [6, 17]. Traditional methods rely on collaborative filtering or shallow content features, whereas recent advances incorporate multimodal signals to enhance item representations. For example, MAPS [7], ECLIP [16], and FAME-VLM [10] exploit product text and images with relatively lightweight, task-specific encoders to generate embeddings. NoteLLM-2 [34] further explores LLM-enhanced multimodal embeddings for retrieval-style I2I recommendation, highlighting the potential of LLMs in industrial retrieval pipelines. However, existing approaches can remain vulnerable to real-world image noise and often lack mechanisms to selectively utilize visual information when it becomes unreliable, leading to brittle nearest-neighbor retrieval in poster-style listings. Our method complements this line by introducing a two-stream, query-based connector with reliability-aware modulation and complementarity regularization, improving robustness and fine-grained retrieval quality in large-scale e-commerce I2I recommendation.

## 3 Preliminary

### 3.1 Problem Formulation

In item-to-item (I2I) retrieval, each item corresponds to a product with a primary image and associated textual metadata. We consider a product set  $\mathcal{I} = \{n_1, n_2, \dots, n_m\}$ , where each product is represented by  $n_i = (v_i, x_i)$ . Here  $v_i$  is the primary product image, and  $x_i$  denotes the textual metadata, which may include a free-form title  $t_i$  and structured fields such as brand  $b_i$  and hierarchical categories  $\mathbf{c}_i = (c_i^{(1)}, c_i^{(2)}, c_i^{(3)})$ .

Given a query product  $n_i$ , the goal is to retrieve a ranked list of relevant items from  $\mathcal{I}$ . We learn an embedding function  $f(\cdot)$  that maps each product to a vector representation  $\mathbf{z}_i = f(v_i, x_i) \in \mathbb{R}^d$ . The relevance between two products is computed by a similarity function (e.g., cosine similarity)  $\text{sim}(\mathbf{z}_i, \mathbf{z}_j)$ , and the system returns items with the highest similarity to the query.

### 3.2 Basic MLRM Pipeline

We follow the standard MLRM pipeline in Fig. 1(b). Given an item  $n_i = (v_i, x_i)$ , we encode the image  $v_i$  with a frozen vision encoder  $V_\theta$  (e.g., CLIP) to obtain visual tokens  $\mathbf{H}_{img,i} \in \mathbb{R}^{L_v \times d_v}$ , optionally along with a global image embedding  $\mathbf{f}_{img,i}^{global} \in \mathbb{R}^{d_v}$ . A lightweight connector  $C_\pi$  then extracts a compact set of visual embeddings in the LLM embedding space,  $\mathbf{E}_i^{(v)} \in \mathbb{R}^{L_c \times d_{llm}}$ , where  $d_{llm}$  is the LLM hidden size. A common instantiation of  $C_\pi$  is a query-based connector (e.g., Q-Former [18]), which uses  $L_c$  learnable queries to cross-attend to  $\mathbf{H}_{img,i}$  and summarize the visual content into  $\mathbf{E}_i^{(v)}$ .

**Prompt-based multimodal injection.** To obtain a single-vector representation suitable for high-throughput retrieval, we inject  $\mathbf{E}_i^{(v)}$  into an LLM prompt. Concretely, we construct a textual prompt from metadata fields in  $x_i$  and reserve a special placeholder token  $\langle \text{IMG} \rangle$  for visual embeddings:

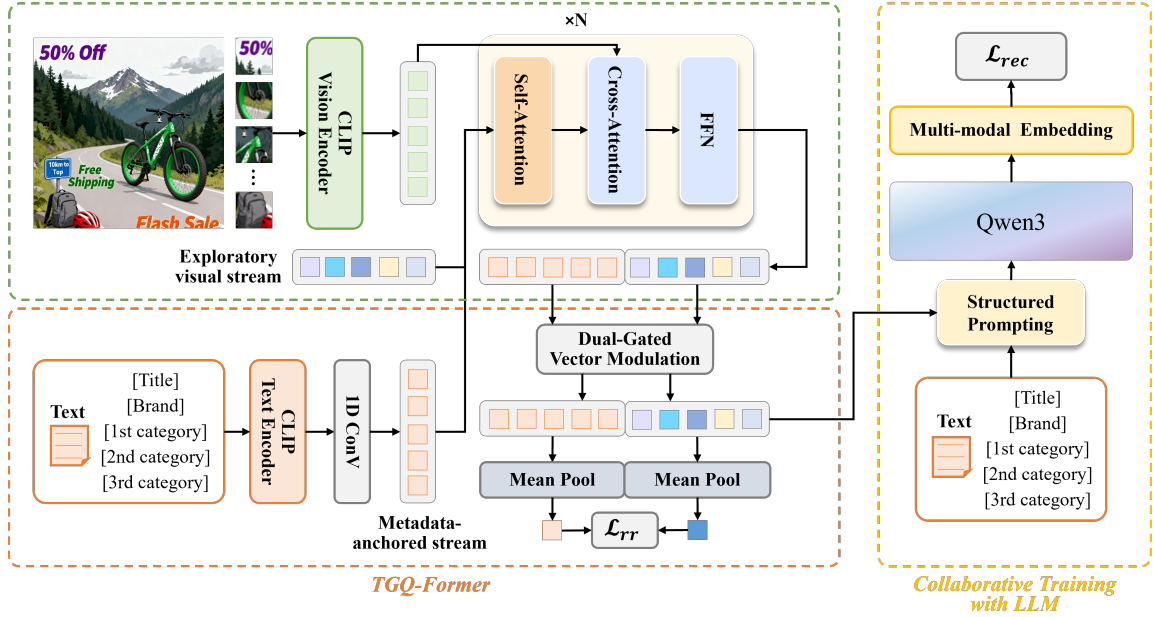


Figure 3: Architecture of the proposed Text-Guided Visual Representation Learning framework.

**Prompt:** Product image: {‘image’: <IMG>}, Product metadata: {‘brand’:  $b_i$ , ‘category’:  $c_i$ , ‘title’:  $t_i$ }. Produce a single embedding for retrieval.

After the LLM token embedding layer, the prompt yields text embeddings  $E_i^{(t)} \in \mathbb{R}^{T \times d_{llm}}$ . We replace the placeholder token at the predefined <IMG> position with the visual embedding sequence  $E_i^{(v)}$ , resulting in a fused multimodal sequence  $E_i^{(m)} \in \mathbb{R}^{(T-1+L_e) \times d_{llm}}$ . The LLM processes  $E_i^{(m)}$  to produce hidden states, and we take the hidden state at a designated summary position (e.g., the last token) as the final item representation  $z_i$ .

**Instantiation in this work.** In TGQ-Former, we instantiate  $C_\pi$  as a *Hybrid-Query Connector (HQC)* that produces two complementary visual embedding streams, i.e., metadata-anchored stream and exploratory stream. A *Dual-Gated Vector Modulation* module then calibrates the two streams before they are injected into the LLM through the <IMG> placeholder (Fig. 3).

## 4 Method

We study item-to-item (I2I) retrieval in e-commerce, where each item  $n_i = (v_i, x_i)$  is associated with an image  $v_i$  and textual metadata  $x_i$  (e.g., title, brand, and hierarchical categories). A practical challenge is that images from poster-style listings often contain promotional overlay artifacts and background clutter, which can introduce spurious cues if visual evidence is fused indiscriminately. Therefore, our key design principle is *adaptive disentanglement*: we extract two complementary streams of visual evidence and calibrate their contributions based on reliability.

Concretely, we disentangle visual evidence into (i) *metadata-anchored semantic evidence* guided by structured metadata, which

helps focus on product-relevant regions and suppress overlay artifacts, and (ii) *exploratory visual evidence* that captures complementary appearance and presentation cues beyond explicit textual metadata. We then *adaptively modulate* the two streams using image-metadata agreement and visual reliability signals.

TGQ-Former consists of three components: (1) a **Hybrid-Query Connector** that produces two complementary sets of LLM-aligned visual tokens (metadata-anchored vs. exploratory); (2) **Dual-Gated Vector Modulation** that performs reliability-aware, channel-wise calibration using a centered-sigmoid gate; and (3) a **Redundancy-Reduction Regularizer** to encourage complementarity.

### 4.1 Hybrid-Query Connector

TGQ-Former extracts retrieval-oriented visual evidence from noisy e-commerce images by combining a metadata-anchored stream and an exploratory stream. Given an item  $n_i = (v_i, x_i)$  with image  $v_i$  and textual metadata  $x_i$ , we use a frozen CLIP vision encoder to obtain visual tokens and a global image embedding. For clarity, we omit the item index  $i$  when the context is unambiguous:

$$H_{img} = \text{CLIP}_{vis}(v) \in \mathbb{R}^{L_v \times d_v}, \quad \mathbf{f}_{img}^{global} = \text{Pool}(H_{img}) \in \mathbb{R}^{d_v}, \quad (1)$$

where  $\text{Pool}(\cdot)$  denotes the encoder’s global pooling (e.g., CLS token or average pooling). We also encode textual metadata with a frozen CLIP text encoder to obtain token embeddings:

$$H_{txt} = \text{CLIP}_{txt}(x) \in \mathbb{R}^{L_t \times d_v}. \quad (2)$$

**Metadata-guided semantic query initialization.** Unlike BLIP-2’s vanilla Q-Former that uses learnable queries without domain-specific priors, we initialize a subset of queries from item metadata

to provide semantic anchors for I2I retrieval. Concretely, we compress  $\mathbf{H}_{txt}$  into a fixed number of query slots using a 1D convolutional downsampling layer:

$$\tilde{\mathbf{H}}_{txt} = \text{Conv1D}(\mathbf{H}_{txt}; k, s) \in \mathbb{R}^{T_g \times d_o}, \quad (3)$$

where  $k$  is the kernel size and  $s$  is the stride. We set  $T_g = \lceil \frac{L_t}{s} \rceil$  (after padding if needed), yielding a deterministic number of semantic query slots. We then project the compressed embeddings into the query space:

$$\mathbf{Q}_{txt} = \tilde{\mathbf{H}}_{txt} \mathbf{W}_Q \in \mathbb{R}^{T_g \times d_q}, \quad (4)$$

where  $\mathbf{W}_Q \in \mathbb{R}^{d_o \times d_q}$  is learnable. The resulting  $\mathbf{Q}_{txt}$  provides metadata-anchored semantic priors for steering cross-attention toward product-relevant regions in poster-style listings.

**Learnable exploratory queries.** To capture complementary visual evidence beyond explicit textual metadata (e.g., fine-grained appearance and presentation cues), we introduce an additional set of learnable queries  $\mathbf{Q}_{rnd} \in \mathbb{R}^{T_r \times d_q}$  initialized randomly.

**Hybrid-Query Connector.** We concatenate the two query sets as the connector input,  $\mathbf{Q}_{in} = [\mathbf{Q}_{txt}; \mathbf{Q}_{rnd}] \in \mathbb{R}^{(T_g+T_r) \times d_q}$ , and feed them into a Q-Former-style **Hybrid-Query Connector** that applies self-attention over queries and cross-attention over visual tokens:

$$\mathbf{E}^{(v)} = [\mathbf{E}_v^{txt}; \mathbf{E}_v^{rnd}] = \text{HQC}(\mathbf{Q}_{in}, \mathbf{H}_{img}), \quad (5)$$

where  $\mathbf{E}_v^{txt} \in \mathbb{R}^{T_g \times d_{llm}}$  denotes metadata-anchored visual embeddings and  $\mathbf{E}_v^{rnd} \in \mathbb{R}^{T_r \times d_{llm}}$  denotes exploratory visual embeddings aligned to the downstream LLM hidden size  $d_{llm}$ .

## 4.2 Dual-Gated Vector Modulation

Images from poster-style listings exhibit diverse noise patterns: promotional overlay artifacts and background clutter can dominate visually salient regions, and the usefulness of metadata anchoring can vary across items due to cross-modal disagreement. To make the two evidence streams robust in such conditions, we introduce a dual-gated, channel-wise modulation module that calibrates the metadata-anchored stream and the exploratory stream *separately*. Unlike scalar gating, our gates output feature-wise vectors to enable *partial trust*: unreliable channels can be suppressed while informative channels are preserved.

**Agreement signal from product titles.** We estimate cross-modal agreement using the product title text, which provides concise, item-specific semantics. Let  $\mathcal{T}^{title}$  denote the title of the current item. We obtain a global title embedding with the frozen CLIP text encoder:

$$\mathbf{f}_{title}^{global} = \text{Pool}(\text{CLIP}_{txt}(\mathcal{T}^{title})) \in \mathbb{R}^{d_o}, \quad (6)$$

and define the image–title agreement score as

$$S_{title} = \cos(\mathbf{f}_{img}^{global}, \mathbf{f}_{title}^{global}) \in [-1, 1]. \quad (7)$$

**Stream summaries.** Given TQG-Former outputs  $\mathbf{E}_v^{txt} \in \mathbb{R}^{T_g \times d_{llm}}$  and  $\mathbf{E}_v^{rnd} \in \mathbb{R}^{T_r \times d_{llm}}$ , we summarize each stream by mean pooling:

$$\bar{\mathbf{e}}_{txt} = \text{Mean}(\mathbf{E}_v^{txt}) \in \mathbb{R}^{d_{llm}}, \quad \bar{\mathbf{e}}_{rnd} = \text{Mean}(\mathbf{E}_v^{rnd}) \in \mathbb{R}^{d_{llm}}. \quad (8)$$

**Vector gate parameterization.** We parameterize channel-wise gates with a centered sigmoid,

$$\text{cSigmoid}(\mathbf{x}) = 2\sigma(\mathbf{x}) - 1 \in (-1, 1), \quad (9)$$

and denote the resulting gate vector as  $\boldsymbol{\beta} \in (-1, 1)^{d_{llm}}$ . We apply residual rescaling  $(1 + \boldsymbol{\beta}) \in (0, 2)^{d_{llm}}$  to each token embedding (broadcast over the token dimension), enabling smooth attenuation or amplification per channel.

**Gating networks.** Both gates are implemented as lightweight two-layer MLPs that map their inputs to a  $d_{llm}$ -dimensional vector:

$$\mathcal{G}_*(\mathbf{u}) = \mathbf{W}_2 \phi(\mathbf{W}_1 \mathbf{u}) \in \mathbb{R}^{d_{llm}}, \quad (10)$$

where  $* \in \{txt, rnd\}$ ,  $\phi(\cdot)$  is a non-linear activation (e.g., GELU), and  $\mathbf{W}_1, \mathbf{W}_2$  are learnable parameters. We use separate parameter sets for  $\mathcal{G}_{txt}$  and  $\mathcal{G}_{rnd}$ .

**Gate for metadata-anchored semantics.** The metadata-anchored stream should be emphasized when the image agrees with textual metadata and down-weighted when the agreement is low. We therefore condition its gate on both the agreement signal and cross-stream context:

$$\mathbf{u}_{txt} = [\mathbf{f}_{img}^{global}; \mathbf{f}_{title}^{global}; S_{title}; \bar{\mathbf{e}}_{txt}; \bar{\mathbf{e}}_{rnd}], \quad (11)$$

$$\boldsymbol{\beta}_{txt} = \text{cSigmoid}(\mathcal{G}_{txt}(\mathbf{u}_{txt})) \in (-1, 1)^{d_{llm}}, \quad (12)$$

$$\tilde{\mathbf{E}}_v^{txt} = \mathbf{E}_v^{txt} \odot (1 + \boldsymbol{\beta}_{txt}). \quad (13)$$

**Gate for exploratory evidence.** The exploratory stream is beneficial for capturing complementary appearance cues, but it can also propagate spurious patterns under severe overlay artifacts in poster-style listings. We thus condition its gate on image-derived and stream-specific signals:

$$\mathbf{u}_{rnd} = [\mathbf{f}_{img}^{global}; \bar{\mathbf{e}}_{rnd}], \quad (14)$$

$$\boldsymbol{\beta}_{rnd} = \text{cSigmoid}(\mathcal{G}_{rnd}(\mathbf{u}_{rnd})) \in (-1, 1)^{d_{llm}}, \quad (15)$$

$$\tilde{\mathbf{E}}_v^{rnd} = \mathbf{E}_v^{rnd} \odot (1 + \boldsymbol{\beta}_{rnd}). \quad (16)$$

Finally, we concatenate the calibrated embeddings and inject them into the downstream LLM:

$$\mathbf{E}^{(v)} = [\tilde{\mathbf{E}}_v^{txt}; \tilde{\mathbf{E}}_v^{rnd}] \in \mathbb{R}^{(T_g+T_r) \times d_{llm}}. \quad (17)$$

## 4.3 Redundancy Reduction for Complementarity

To encourage the metadata-anchored stream and the exploratory stream to encode complementary evidence, we adopt a redundancy reduction objective over each mini-batch. For each item  $i$  in a batch of size  $B$ , we pool the calibrated embeddings into stream-level vectors:

$$\mathbf{s}_i^{txt} = \text{Mean}(\tilde{\mathbf{E}}_{v,i}^{txt}) \in \mathbb{R}^{d_{llm}}, \quad \mathbf{s}_i^{rnd} = \text{Mean}(\tilde{\mathbf{E}}_{v,i}^{rnd}) \in \mathbb{R}^{d_{llm}}. \quad (18)$$

Stacking them across the batch yields matrices  $\mathbf{S}^{txt} = [\mathbf{s}_1^{txt}; \dots; \mathbf{s}_B^{txt}] \in \mathbb{R}^{B \times d_{llm}}$  and  $\mathbf{S}^{rnd} = [\mathbf{s}_1^{rnd}; \dots; \mathbf{s}_B^{rnd}] \in \mathbb{R}^{B \times d_{llm}}$ .

We standardize each feature dimension across the mini-batch:

$$\hat{\mathbf{S}}^{txt} = \frac{\mathbf{S}^{txt} - \text{Mean}_B(\mathbf{S}^{txt})}{\text{Std}_B(\mathbf{S}^{txt}) + \epsilon}, \quad \hat{\mathbf{S}}^{rnd} = \frac{\mathbf{S}^{rnd} - \text{Mean}_B(\mathbf{S}^{rnd})}{\text{Std}_B(\mathbf{S}^{rnd}) + \epsilon}, \quad (19)$$

where  $\text{Mean}_B(\cdot)$  and  $\text{Std}_B(\cdot)$  are computed per feature dimension over the batch.

We then compute the cross-correlation matrix between the two streams:

$$\mathbf{C} = \frac{1}{B} (\hat{\mathbf{S}}^{txt})^\top \hat{\mathbf{S}}^{rnd} \in \mathbb{R}^{d_{llm} \times d_{llm}}. \quad (20)$$

The redundancy reduction loss penalizes same-dimension cross-stream correlations:

$$\mathcal{L}_{rr} = \frac{1}{d_{llm}} \|\text{diag}(\mathbf{C})\|_2^2 = \frac{1}{d_{llm}} \sum_{k=1}^{d_{llm}} C_{kk}^2, \quad (21)$$

which discourages the two streams from encoding redundant evidence in the same subspace while allowing useful cross-dimension interactions.

#### 4.4 Joint Contrastive Training for I2I Retrieval

Following the MLRM prompting interface, we inject the calibrated visual embeddings  $\mathbf{E}^{(v)} = [\tilde{\mathbf{E}}_v^{txt}; \tilde{\mathbf{E}}_v^{rnd}]$  into a pretrained LLM together with the metadata prompt (by replacing the <IMG> placeholder), and obtain an item representation  $\mathbf{z}_i$  from the LLM hidden states (e.g., the last-token hidden state). We train the model for retrieval-style I2I recommendation with an InfoNCE-style contrastive objective over positive item pairs  $(i, j)$  and in-batch negatives:

$$\mathcal{L}_{rec} = -\log \frac{\exp(\text{sim}(\mathbf{z}_i, \mathbf{z}_j)/\tau)}{\sum_{k \in \mathcal{B} \setminus \{i\}} \exp(\text{sim}(\mathbf{z}_i, \mathbf{z}_k)/\tau)}, \quad (22)$$

where  $\mathcal{B}$  denotes the current mini-batch,  $\text{sim}(\cdot, \cdot)$  is cosine similarity, and  $\tau$  is the temperature.

The overall training objective is

$$\mathcal{L} = \mathcal{L}_{rec} + \lambda_{rr} \mathcal{L}_{rr}. \quad (23)$$

## 5 Experiments

To systematically evaluate the effectiveness of our proposed framework, we conduct comprehensive experiments designed to answer the following research questions (RQs):

- **RQ1:** How does our overall framework perform compared to state-of-the-art multimodal recommendation methods and existing connector designs?
- **RQ2:** How does our TGQ-Former-based MLRM paradigm compare with directly applying end-to-end MLLMs in terms of both retrieval quality and computational efficiency?
- **RQ3:** What are the individual contributions of the Hybrid-Query Connector, Dual-Gated Vector Modulation, and the Redundancy-Reduction Regularizer?
- **RQ4:** How do metadata-anchored and exploratory queries allocate cross-attention over visual regions in poster-style listings?

### 5.1 Experiments Setup

**5.1.1 Datasets.** We construct our dataset from one year of user “add-to-cart” behavior logs sourced from the Checkout Page Add-on channel of our e-commerce platform. To generate candidate item pairs, we employ the Swing algorithm [32] to recall the top-100 similar items for each trigger item. Note that Swing is only used for constructing training/testing pairs; during evaluation, we perform full-pool retrieval over all test items (about 134K candidates) for every query. The final dataset contains approximately 3.5 million item pairs for training and 67,000 for testing. To prevent data leakage, the trigger items in the training and testing sets are strictly disjoint, with both sets exhibiting similar data distributions. Detailed dataset statistics are provided in Table 1.

**Table 1: Detailed statistics of training and testing datasets.**

Training Dataset			
item pairs	3,521,865	unique items	148,270
avg. words per sku title	46.85	1st categories	54
avg. words per sku brand	5.66	2nd categories	466
		3rd categories	2820
Testing Dataset			
item pairs	67,341	unique items	134,682
avg. words per sku title	48.02	1st categories	51
avg. words per sku brand	5.40	2nd categories	419
		3rd categories	2096

**5.1.2 Baselines.** We compare with representative *connector/fusion designs* that have been widely used to bridge frozen vision encoders and LLMs in MLLM/MLRM literature:

- **LLaVA:Linear** [22]: a single linear projection that maps visual features into the LLM embedding space.
- **LLaVA-1.5:MLP** [21]: a two-layer MLP for non-linear feature transformation.
- **Perceiver-Resampler** (Flamingo-style) [1]: a perceiver-resampler module that compresses and aligns visual tokens with language inputs.

We further include recent multimodal retrieval/recommendation methods with similar MLRM-style pipelines:

- **NoteLLM-2** [34]: a BLIP-2 Q-Former based connector with design choices tailored for retrieval-style recommendation.
- **EM3** [8]: an FQ-Former that uses trainable queries and Trans-former layers to fuse vision and text into fixed-length embeddings.
- **UniECS** [20]: a gated cross-modal fusion mechanism originally proposed for e-commerce search; we adapt it to our I2I setting for comparison.

**5.1.3 Metrics.** We evaluate I2I retrieval using Hit Rate (H@K) [24] at  $K \in \{1, 5, 10, 20, 50, 100\}$ . For each query item  $i$  in the test set, we rank *all* candidate items in the test item pool (approximately 134K unique items) by cosine similarity between their learned embeddings. H@K is computed as whether at least one ground-truth positive item of  $i$  appears in the top- $K$  ranked list. All methods are evaluated under the same full-pool retrieval protocol.

**5.1.4 Implementation Details.** We implement all models in PyTorch and train them with DDP on up to 8 H100 GPUs. Unless otherwise noted, all methods use the same frozen Chinese-CLIP-ViT-B/16 [30] visual encoder and the same Qwen3-Embedding-0.6B [36] backbone in the prompting pipeline. We train with an InfoNCE objective and obtain a 256-dimensional item embedding via a linear projection from the LLM hidden state at the designated summary position. Additional details are deferred to Appendix B.

### 5.2 Overall Performance Evaluation (RQ1)

We evaluate the overall I2I retrieval performance of our framework against the baselines in Sec. 5.1.2. All methods share the same vision encoder, prompting interface, and contrastive training objective; only the connector/fusion module differs. We report

**Table 2: Comparison of modality fusion methods across three different LLMs.**

Base Model	Connector	H@1	H@5	H@10	H@20	H@50	H@100
Chinese-CLIP-ViT-B/16 + Qwen3-Embedding-0.6B	LLaVA:linear	7.86	20.16	27.73	37.18	51.08	62.11
	LLaVA1.5:MLP	7.80	20.09	27.60	37.01	51.27	61.81
	Perceiver-Resampler	8.04	21.58	29.36	39.23	53.22	63.97
	EM3	5.20	13.48	19.74	28.13	42.58	55.63
	UniECS	6.60	17.85	25.07	34.30	48.95	60.76
	NoteLLM-2	8.19	21.54	29.83	39.60	54.36	65.19
	TGQ-Former (Ours)	<b>8.44</b>	<b>22.18</b>	<b>31.62</b>	<b>42.93</b>	<b>58.58</b>	<b>69.13</b>
Chinese-CLIP-ViT-B/16 + Qwen3-1.7B	LLaVA:linear	7.77	20.38	27.99	37.33	51.17	62.17
	LLaVA1.5:MLP	7.68	20.22	28.02	37.46	51.63	62.29
	Perceiver-Resampler	7.92	<b>20.59</b>	<b>28.39</b>	37.43	51.46	62.10
	EM3	3.83	11.06	16.12	23.35	36.93	49.87
	UniECS	6.84	17.85	24.87	34.02	48.49	59.77
	NoteLLM-2	7.91	20.45	28.06	<u>37.73</u>	<u>52.10</u>	<u>62.92</u>
	TGQ-Former (Ours)	<b>8.13</b>	<u>20.53</u>	<u>28.34</u>	<b>38.05</b>	<b>52.36</b>	<b>63.20</b>
Chinese-CLIP-ViT-B/16 + Baichuan2-7B-Chat	LLaVA:linear	7.53	19.64	27.14	36.51	50.77	61.68
	LLaVA1.5:MLP	7.53	19.89	27.41	36.55	50.93	61.91
	Perceiver-Resampler	7.87	20.26	27.89	37.37	51.77	62.46
	EM3	4.40	12.42	18.41	26.80	41.48	54.57
	UniECS	7.50	19.87	27.84	37.83	52.64	63.85
	NoteLLM-2	8.07	20.95	29.16	39.04	53.55	64.19
	TGQ-Former (Ours)	<b>8.18</b>	<b>21.34</b>	<b>29.40</b>	<b>39.36</b>	<b>54.07</b>	<b>64.57</b>

results with three backbones in the MLRM prompting pipeline: Qwen3-Embedding-0.6B [36], Qwen3-1.7B [29], and Baichuan2-7B-Chat [31], to assess generalizability across model families (details in Appendix Table 5). For Qwen3-1.7B and Baichuan2-7B-Chat, we follow common practice [34, 36] and use the hidden state at the designated summary position (e.g., the last token) as the item embedding.

Table 2 shows that our method consistently outperforms all baselines across  $K \in \{1, 5, 10, 20, 50, 100\}$  under the full-pool retrieval protocol over the  $\sim 134K$  test candidates. With the Qwen3-Embedding-0.6B backbone, our model improves H@100 from 65.19 (NoteLLM-2) to 69.13, corresponding to +3.94 absolute points (6.04% relative). Compared with the Perceiver-Resampler connector, we achieve +5.16 absolute points at H@100 (8.07% relative). Improvements over linear/MLP connectors are also substantial, indicating that query-based tokenization with reliability-aware calibration is more effective for our noisy e-commerce imagery than directly projecting dense visual features.

Across backbones, we observe that the embedding-oriented Qwen3-Embedding-0.6B consistently yields strong performance, sometimes surpassing larger generative LLM backbones. A plausible explanation is that embedding models are explicitly trained for representation learning and similarity-based retrieval, which better matches the objective of I2I embedding learning.

### 5.3 Performance Comparison with MLLMs (RQ2)

We compare our MLRM framework with end-to-end Multimodal LLMs (MLLMs) that directly encode images and text into a unified embedding. We select representative 2–4B-class open-source

MLLMs, including InternVL3-2B-Instruct [37], Qwen2-VL-2B-Instruct [25], Qwen2.5-VL-3B-Instruct [3] and Qwen3-VL-4B-Instruct [2]. For preprocessing, we follow each model’s recommended configuration: images are resized to  $224 \times 224$  by default, while InternVL3 uses its official  $448 \times 448$  setting. We report both retrieval quality (H@K) under the same full-pool evaluation protocol and the inference compute cost in GFLOPs per item embedding.

**Table 3: The contrast between using MLLMs and using MLRMs with TGQ-Former.**

Model	H@1	H@5	H@10	H@20	H@50	H@100	GFLOPs
<b>Using MLLMs</b>							
InternVL3-2B-Instruct	7.10	18.67	26.40	35.86	50.56	61.83	724.71
Qwen2-VL-2B-Instruct	7.18	18.86	26.33	35.93	50.54	61.59	298.91
Qwen2.5-VL-3B-Instruct	<u>8.48</u>	<u>22.07</u>	<u>30.16</u>	39.89	54.03	64.68	450.16
Qwen3-VL-4B-Instruct	8.10	21.44	29.90	<u>39.98</u>	<u>54.63</u>	<u>65.68</u>	592.23
<b>Using MLRMs with TGQ-Former</b>							
Chinese-CLIP-ViT-B/16 + Qwen3-Embedding-0.6B	8.44	22.18	31.62	42.93	58.58	69.13	35.43

Table 3 shows that our method achieves consistently better retrieval quality than all compared MLLMs while being substantially more compute-efficient. Compared with the strongest MLLM baseline, Qwen3-VL-4B-Instruct, our model improves H@100 from 65.68 to 69.13 (+3.45 absolute points), and also yields gains at other  $K$  values. Meanwhile, our MLRM requires 8–20× fewer GFLOPs (35.43 vs 298–725 GFLOPs), highlighting the advantage of lightweight connectors and retrieval-oriented embedding backbones for high-throughput I2I retrieval.

## 5.4 Ablation Study (RQ3)

We ablate key components of TGQ-Former under the same setting (Chinese-CLIP-ViT-B/16 + Qwen3-Embedding-0.6B) and full-pool retrieval over  $\sim 134\text{K}$  test candidates. Results are reported in Table 4.

**Hybrid-Query Connector.** Starting from a Q-Former baseline with exploratory queries only, replacing them with metadata-anchored semantic queries yields a clear gain, improving  $H@100$  from 65.19 to 67.45. Combining semantic and exploratory queries further improves performance, raising  $H@100$  to 68.11, indicating that the exploratory stream provides complementary cues beyond metadata.

**Dual-Gated Vector Modulation.** Adding Dual-Gated Vector Modulation on top of hybrid queries consistently boosts retrieval quality, improving  $H@100$  from 68.11 to 68.90, supporting the need to calibrate the two streams separately under noisy poster-style listings.

**Redundancy-Reduction Regularizer.** Finally, introducing the Redundancy-Reduction Regularizer brings additional improvement, increasing  $H@100$  from 68.90 to 69.13. Overall, the full model achieves the best results, demonstrating that hybrid queries, dual-gated calibration, and redundancy reduction contribute additively to robust I2I retrieval.

## 5.5 Qualitative Analysis of Disentangled Queries (RQ4)

To qualitatively examine how TGQ-Former disentangles metadata-anchored and exploratory visual evidence in poster-style listings, we visualize cross-attention maps on selected test examples. Specifically, we extract the multi-head cross-attention weights from the last HQC layer and average them over attention heads. Fig. 4 compares the attended regions of metadata-anchored semantic queries and exploratory queries.

As shown in Fig. 4, semantic queries typically focus on product-relevant regions that are consistent with the metadata semantics, while largely avoiding visually salient but product-irrelevant overlay artifacts and decorative layouts. In contrast, exploratory queries exhibit more diverse attention patterns, capturing both global context and fine-grained appearance cues that may not be explicitly specified by metadata. These qualitative patterns are consistent with the intended roles of the two query streams.

We also observe complementary behavior in challenging cases. When semantic queries attend to less informative regions in some cases, exploratory queries may still localize product-relevant evidence, providing complementary signals beyond metadata anchoring.

Fig. 5 further illustrates examples with dense promotional overlays and clutter. Even when high-contrast overlays occupy large portions of the image, semantic queries tend to localize product-relevant regions more consistently, while exploratory queries capture broader appearance patterns that can complement metadata-guided extraction.

## 6 Conclusion

This paper studied multimodal item-to-item (I2I) retrieval in e-commerce, where poster-style images often contain promotional

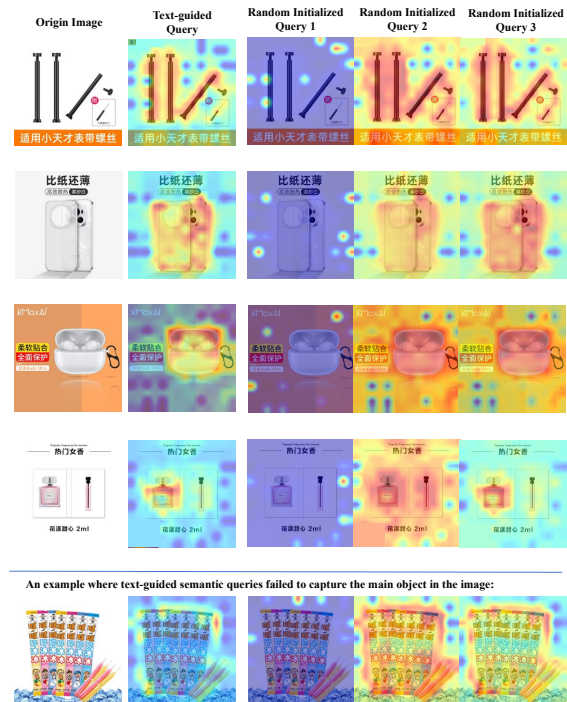


**Figure 4: Cross-attention visualization of different query types in TGQ-Former.** Each row corresponds to one product image. The first column shows the original image. The second column shows the averaged cross-attention map of metadata-anchored semantic queries (averaged over queries and heads). The third to fifth columns show cross-attention maps of three representative exploratory queries, respectively.



**Figure 5: Qualitative examples from poster-style listings with dense overlay artifacts and clutter.** For each item, we show the original image (left), the averaged cross-attention map of metadata-anchored semantic queries (middle), and the averaged map of exploratory queries (right).

overlays and clutter, introducing spurious cues and degrading fine-grained retrieval. We proposed TGQ-Former, a text-guided framework that performs *adaptive disentanglement* by producing two

**Table 4: Ablation study of our framework. All variants share the same vision encoder and LLM backbone; only the connector/modulation components differ.**

Variant	Metadata-anchored Queries	Exploratory Queries	Gating	$\mathcal{L}_{rr}$	H@20	H@50	H@100
(a) Q-Former(Exploratory-only)	–	✓	–	–	39.60	54.36	65.19
(b) Metadata-anchored-only	✓	–	–	–	41.73	56.45	67.45
(c) Hybrid queries	✓	✓	–	–	42.30	57.32	68.11
(d) + Dual-gated Vector Modulation	✓	✓	✓	–	42.77	58.01	68.90
(e) + Dual-Gate + RR (full)	✓	✓	✓	✓	<b>42.93</b>	<b>58.58</b>	<b>69.13</b>

complementary visual streams: metadata-anchored semantic queries capture metadata-consistent evidence, while exploratory queries capture complementary patterns beyond explicit metadata. To improve robustness under heterogeneous noise, we introduced Dual-Gated Vector Modulation to calibrate the streams using cross-modal agreement and image-derived cues, and a Redundancy-Reduction Regularizer to encourage complementarity. Experiments on a large-scale real-world dataset with full-pool retrieval show consistent gains over strong connector baselines and end-to-end MLLMs at substantially lower inference compute.

## References

- Jean-Baptiste Alayrac, Jeff Donahue, Pauline Luc, Antoine Miech, Iain Barr, Yana Hasson, Karel Lenc, Arthur Mensch, Katherine Millican, Malcolm Reynolds, et al. 2022. Flamingo: a visual language model for few-shot learning. *Advances in neural information processing systems* 35 (2022), 23716–23736.
- Shuai Bai, Yuxuan Cai, Ruizhe Chen, Keqin Chen, Xiong-Hui Chen, Zesen Cheng, Lianghao Deng, Wei Ding, Rongyao Fang, Chang Gao, Chunjiang Ge, Wenbin Ge, Zhifang Guo, Qidong Huang, Fei Huang, Binyuan Hui, Shutong Jiang, Zhaohai Li, Mingsheng Li, Mei Li, Kaixin Li, Zicheng Lin, Junyang Lin, Xuejing Liu, Jiawei Liu, Chenglong Liu, Yang Liu, Dayiheng Liu, Shixuan Liu, Dunjie Lu, Ruilin Luo, Chenxu Lv, Rui Men, Li Ying Meng, Xuancheng Ren, Xin yi Ren, Sibao Song, Yu-Chen Sun, Jun Tang, Jianhong Tu, Jianqiang Wan, Peng Wang, Pengfei Wang, Qiuyue Wang, Yuxuan Wang, Tianbao Xie, Yihe Xu, Haiyang Xu, Jin Xu, Zhibo Yang, Mingkun Yang, Jianxin Yang, An Yang, Bowen Yu, Fei Zhang, Hang Zhang, Xi Zhang, Botao Zheng, Humen Zhong, Jingren Zhou, Fanxi Zhou, Jingren Zhou, Yuanzhi Zhu, and Keming Zhu. 2025. Qwen3-VL Technical Report. *arXiv abs/2511.21631* (2025).
- Shuai Bai, Keqin Chen, Xuejing Liu, Jialin Wang, Wenbin Ge, Sibao Song, Kai Dang, Peng Wang, Shijie Wang, Jun Tang, et al. 2025. Qwen2.5-vl technical report. *arXiv preprint arXiv:2502.13923* (2025).
- Xu Chen, Hanxiong Chen, Hongteng Xu, Yongfeng Zhang, Yixin Cao, Zheng Qin, and Hongyuan Zha. 2019. Personalized Fashion Recommendation with Visual Explanations based on Multimodal Attention Network: Towards Visually Explainable Recommendation. In *Proceedings of the 42nd International ACM SIGIR Conference on Research and Development in Information Retrieval* (Paris, France) (SIGIR'19). Association for Computing Machinery, New York, NY, USA, 765–774. doi:10.1145/3331184.3331254
- Yen-Chun Chen, Linjie Li, Licheng Yu, Ahmed El Kholy, Faisal Ahmed, Zhe Gan, Yu Cheng, and Jingjing Liu. 2020. UNITER: UNiversal Image-TExt Representation Learning. In *Computer Vision – ECCV 2020: 16th European Conference, Glasgow, UK, August 23–28, 2020, Proceedings, Part XXX* (Glasgow, United Kingdom). Springer-Verlag, Berlin, Heidelberg, 104–120. doi:10.1007/978-3-030-58577-8\_7
- Paul Covington, Jay Adams, and Emre Sargin. 2016. Deep Neural Networks for YouTube Recommendations. In *Proceedings of the 10th ACM Conference on Recommender Systems* (Boston, Massachusetts, USA) (RecSys '16). Association for Computing Machinery, New York, NY, USA, 191–198. doi:10.1145/2959100.2959190
- Nilotpal Das, Aniket Joshi, Promod Yenigalla, and Gourav Agrwal. 2022. MAPS: Multimodal Attention for Product Similarity. In *Proceedings of the IEEE/CVF Winter Conference on Applications of Computer Vision (WACV)*. 3551–3560.
- Xiuqi Deng, Lu Xu, Xiyao Li, Jinkai Yu, Erpeng Xue, Zhongyuan Wang, Di Zhang, Zhaojie Liu, Guorui Zhou, Yang Song, et al. 2024. End-to-End Training of Multimodal Model and Ranking Model. *arXiv preprint arXiv:2404.06078* (2024).
- Karan Desai and Justin Johnson. 2021. VirTex: Learning Visual Representations from Textual Annotations. In *2021 IEEE/CVF Conference on Computer Vision and Pattern Recognition (CVPR)*. IEEE Computer Society, Los Alamitos, CA, USA, 11157–11168. doi:10.1109/CVPR46437.2021.01101
- Xiao Han, Xiatian Zhu, Licheng Yu, Li Zhang, Yi-Zhe Song, and Tao Xiang. 2023. FAME-ViL: Multi-Tasking Vision-Language Model for Heterogeneous Fashion Tasks. *2023 IEEE/CVF Conference on Computer Vision and Pattern Recognition (CVPR)* (2023), 2669–2680.
- Yupeng Hou, Junjie Zhang, Zihan Lin, Hongyu Lu, Ruobing Xie, Julian McAuley, and Wayne Xin Zhao. 2024. Large Language Models are Zero-Shot Rankers for Recommender Systems. In *Advances in Information Retrieval: 46th European Conference on Information Retrieval, ECIR 2024, Glasgow, UK, March 24–28, 2024, Proceedings, Part II* (Glasgow, United Kingdom). Springer-Verlag, Berlin, Heidelberg, 364–381. doi:10.1007/978-3-031-56060-6\_24
- Andrew Jaegle, Sebastian Borgeaud, Jean-Baptiste Alayrac, Carl Doersch, Catalin Ionescu, David Ding, Skanda Koppula, Andrew Zisserman, Oriol Vinyals, and Joao Carreira. 2022. Perceiver IO: A General Architecture for Structured Inputs & Outputs. In *International Conference on Learning Representations (ICLR)*, Vol. abs/2107.14795.
- Andrew Jaegle, Felix Gimeno, Andrew Brock, Andrew Zisserman, Oriol Vinyals, and Joao Carreira. 2021. Perceiver: General Perception with Iterative Attention. In *Proceedings of the 38th International Conference on Machine Learning (ICML) (Proceedings of Machine Learning Research, Vol. 139)*, Marina Meila and Tong Zhang (Eds.). PMLR, 4651–4664. <http://proceedings.mlr.press>
- Chao Jia, Yinfei Yang, Ye Xia, Yi-Ting Chen, Zarana Parekh, Hieu Pham, Quoc V. Le, Yun-Hsuan Sung, Zhen Li, and Tom Duerig. 2021. Scaling Up Visual and Vision-Language Representation Learning With Noisy Text Supervision. In *Proceedings of the 38th International Conference on Machine Learning, ICM 2021, 18–24 July 2021, Virtual Event (Proceedings of Machine Learning Research, Vol. 139)*, Marina Meila and Tong Zhang (Eds.). PMLR, 4904–4916. <http://proceedings.mlr.press/v139/jia21b.html>
- Yiren Jian, Chongyang Gao, and Soroush Vosoughi. 2023. Bootstrapping vision-language learning with decoupled language pre-training. In *Proceedings of the 37th International Conference on Neural Information Processing Systems* (New Orleans, LA, USA) (NIPS '23). Curran Associates Inc., Red Hook, NY, USA, Article 4, 16 pages.
- Yang Jin, Yongzhi Li, Zehuan Yuan, and Yadong Mu. 2023. Learning Instance-Level Representation for Large-Scale Multi-Modal Pretraining in E-Commerce. *2023 IEEE/CVF Conference on Computer Vision and Pattern Recognition (CVPR)* (2023), 11060–11069.
- Jeff Johnson, Matthijs Douze, and Hervé Jégou. 2017. Billion-scale similarity search with GPUs. *CoRR abs/1702.08734* (2017). <http://dblp.uni-trier.de/db/journals/corr/corr1702.html#JohnsonD17>
- Junnan Li, Dongxu Li, Silvio Savarese, and Steven Hoi. 2023. Blip-2: Bootstrapping language-image pre-training with frozen image encoders and large language models. In *International conference on machine learning*. PMLR, 19730–19742.
- Xiujun Li, Xi Yin, Chunyuan Li, Pengchuan Zhang, Xiaowei Hu, Lei Zhang, Lijuan Wang, Houdong Hu, Li Dong, Furu Wei, Yejin Choi, and Jianfeng Gao. 2020. Oscar: Object-Semantics Aligned Pre-training for Vision-Language Tasks. In *Computer Vision – ECCV 2020: 16th European Conference, Glasgow, UK, August 23–28, 2020, Proceedings, Part XXX* (Glasgow, United Kingdom). Springer-Verlag, Berlin, Heidelberg, 121–137. doi:10.1007/978-3-030-58577-8\_8
- Zihan Liang, Yufei Ma, Zhipeng Qian, Huangyu Dai, Zihan Wang, Ben Chen, Chenyi Lei, Yuqing Ding, and Han Li. 2025. UniECS: Unified Multimodal E-Commerce Search Framework with Gated Cross-modal Fusion. In *Proceedings of the 34th ACM International Conference on Information and Knowledge Management* (Seoul, Republic of Korea) (CIKM '25). Association for Computing Machinery, New York, NY, USA, 1788–1797. doi:10.1145/3746252.3761170
- Haotian Liu, Chunyuan Li, Yuheng Li, and Yong Jae Lee. 2024. Improved baselines with visual instruction tuning. In *Proceedings of the IEEE/CVF conference on computer vision and pattern recognition*. 26296–26306.
- Haotian Liu, Chunyuan Li, Qingyang Wu, and Yong Jae Lee. 2023. Visual Instruction Tuning. In *Advances in Neural Information Processing Systems*, A. Oh, T. Naumann, A. Globerson, K. Saenko, M. Hardt, and S. Levine (Eds.), Vol. 36. Curran Associates, Inc., 34892–34916. [https://proceedings.neurips.cc/paper\\_files/paper/2023/file/6dcf277ea32ce3288914faf369f6e6d0-Paper-Conference.pdf](https://proceedings.neurips.cc/paper_files/paper/2023/file/6dcf277ea32ce3288914faf369f6e6d0-Paper-Conference.pdf)

- [23] Alec Radford, Jong Wook Kim, Chris Hallacy, Aditya Ramesh, Gabriel Goh, Sandhini Agarwal, Girish Sastry, Amanda Askell, Pamela Mishkin, Jack Clark, Gretchen Krueger, and Ilya Sutskever. 2021. Learning Transferable Visual Models From Natural Language Supervision. In *Proceedings of the 38th International Conference on Machine Learning, ICML 2021, 18–24 July 2021, Virtual Event (Proceedings of Machine Learning Research, Vol. 139)*, Marina Meila and Tong Zhang (Eds.). PMLR, 8748–8763. <http://proceedings.mlr.press/v139/radford21a.html>
- [24] Yan-Martin Tamm, Rinchin Dandinov, and Alexey Vasilev. 2021. Quality metrics in recommender systems: Do we calculate metrics consistently?. In *Proceedings of the 15th ACM conference on recommender systems*. 708–713.
- [25] Peng Wang, Shuai Bai, Sinan Tan, Shijie Wang, Zhihao Fan, Jinze Bai, Keqin Chen, Xuejing Liu, Jialin Wang, Wenbin Ge, et al. 2024. Qwen2-vl: Enhancing vision-language model’s perception of the world at any resolution. *arXiv preprint arXiv:2409.12191* (2024).
- [26] Yinwei Wei, Xiang Wang, Liqiang Nie, Xiangnan He, Richang Hong, and Tat-Seng Chua. 2019. MMGCN: Multi-modal Graph Convolution Network for Personalized Recommendation of Micro-video. In *Proceedings of the 27th ACM International Conference on Multimedia (Nice, France) (MM ’19)*. Association for Computing Machinery, New York, NY, USA, 1437–1445. doi:10.1145/334031.3351034
- [27] Likang Wu, Zhi Zheng, Zhaopeng Qiu, Hao Wang, Hongchao Gu, Tingjia Shen, Chuan Qin, Chen Zhu, Hengshu Zhu, Qi Liu, Hui Xiong, and Enhong Chen. 2024. A survey on large language models for recommendation. *World Wide Web* 27, 5 (Aug. 2024), 31 pages. doi:10.1007/s11280-024-01291-2
- [28] Jinfeng Xu, Zheyu Chen, Shuo Yang, Jinze Li, Wei Wang, Xiping Hu, Steven Hoi, and Edith C. H. Ngai. 2025. A Survey on Multimodal Recommender Systems: Recent Advances and Future Directions. *ArXiv abs/2502.15711* (2025).
- [29] An Yang, Anfeng Li, Baosong Yang, Beichen Zhang, Binyuan Hui, Bo Zheng, Bowen Yu, Chang Gao, Chengen Huang, Chenxu Lv, et al. 2025. Qwen3 technical report. *arXiv preprint arXiv:2505.09388* (2025).
- [30] An Yang, Junshu Pan, Junyang Lin, Rui Men, Yichang Zhang, Jingren Zhou, and Chang Zhou. 2022. Chinese clip: Contrastive vision-language pretraining in chinese. *arXiv preprint arXiv:2211.01335* (2022).
- [31] Aiyuan Yang, Bin Xiao, Bingning Wang, Borong Zhang, Ce Bian, Chao Yin, Chenxu Lv, Da Pan, Dian Wang, Dong Yan, et al. 2023. Baichuan 2: Open large-scale language models. *arXiv preprint arXiv:2309.10305* (2023).
- [32] Xiaoyong Yang, Yadong Zhu, Yi Zhang, Xiaobo Wang, and Quan Yuan. 2020. Large scale product graph construction for recommendation in e-commerce. *arXiv preprint arXiv:2010.05525* (2020).
- [33] Lu Yuan, Dongdong Chen, Yi-Ling Chen, Noel Codella, Xiyang Dai, Jianfeng Gao, Houdong Hu, Xuedong Huang, Boxin Li, Chunyuan Li, Ce Liu, Mengchen Liu, Zicheng Liu, Yumao Lu, Yu Shi, Lijuan Wang, Jianfeng Wang, Bin Xiao, Zhen Xiao, Jianwei Yang, Michael Zeng, Luwei Zhou, and Pengchuan Zhang. 2021. Florence: A New Foundation Model for Computer Vision. *ArXiv abs/2111.11432* (2021).
- [34] Chao Zhang, Haoxin Zhang, Shiwei Wu, Di Wu, Tong Xu, Xiangyu Zhao, Yan Gao, Yao Hu, and Enhong Chen. 2025. Notellm-2: Multimodal large representation models for recommendation. In *Proceedings of the 31st ACM SIGKDD Conference on Knowledge Discovery and Data Mining V. 1*. 2815–2826.
- [35] Pengchuan Zhang, Xiujun Li, Xiaowei Hu, Jianwei Yang, Lei Zhang, Lijuan Wang, Choi Yejin, and Jianfeng Gao. 2021. VinVL: Revisiting Visual Representations in Vision-Language Models. In *Proceedings of the IEEE/CVF Conference on Computer Vision and Pattern Recognition (CVPR)*. 5579–5588.
- [36] Yanzhao Zhang, Mingxin Li, Dingkun Long, Xin Zhang, Huan Lin, Baosong Yang, Pengjun Xie, An Yang, Dayiheng Liu, Junyang Lin, et al. 2025. Qwen3 Embedding: Advancing Text Embedding and Reranking Through Foundation Models. *arXiv preprint arXiv:2506.05176* (2025).
- [37] Jinguo Zhu, Weiyun Wang, Zhe Chen, Zhaoyang Liu, Shenglong Ye, Lixin Gu, Hao Tian, Yuchen Duan, Weijie Su, Jie Shao, et al. 2025. Internvl3: Exploring advanced training and test-time recipes for open-source multimodal models. *arXiv preprint arXiv:2504.10479* (2025).

## A Model Details

We present the details of the three LLMs employed in our method in Table 5, and the details of the four MLLMs used for comparative experiments in Table 6. Since our platform is designed for the Chinese market, all selected models provide support for Chinese processing.

Table 5: Model settings of LLMs

Configuration	Qwen3-Embedding-0.6B	Qwen3-1.7B	Baichuan2-7B
# LLM layers	28	28	32
# LLM attention heads	16	16	32
Vocab size	151669	151936	125696
LLM hidden size $d_{llm}$	1024	2048	4096
LLM intermediate size	3072	6144	4864

Table 6: Model settings of MLLMs

Configuration	InternVL3-2B	Qwen2-VL-2B	Qwen2.5-VL-3B	Qwen3-VL-4B
Vision encoder $V_v$	InternViT	ViT	ViT	ViT
Connector $C_\pi$	MLP	MLP	MLP	MLP (vision projector)
LLM $LLM_\mu$	Qwen2.5	Qwen2	Qwen2.5	Qwen3
# Vision encoder layers	24	32	32	24
# Vision encoder attention heads	16	16	16	16
Vision encoder hidden size $h_v$	1024	1536	1280	1024
Vision encoder intermediate size	4096	6144	3456	4096
# LLM layers	28	28	36	36
# LLM attention heads	12	12	16	32
Vocab size	151674	151936	151646	151936
LLM hidden size $d_{llm}$	1536	1536	2048	2560
LLM intermediate size	8960	8960	4864	9728

## B Training Details and Hyperparameters

**Backbones and preprocessing.** We use a frozen CLIP image encoder and CLIP text encoder. Specifically, we use Chinese-CLIP-ViT-B/16 with the standard CLIP preprocessing: images are resized and center-cropped to  $224 \times 224$  and normalized with the CLIP mean/std. Item titles are tokenized with the CLIP tokenizer, truncated to 50 tokens. The LLM backbone is Qwen3-Embedding-0.6B; we use its default tokenizer with a maximum length of 8192 tokens. Unless stated otherwise, no additional image or text augmentation is applied.

**Training.** We train HQC and the dual-gating modules, and apply LoRA to the LLM backbone (only LoRA parameters are trainable in the LLM). We use AdamW with the hyperparameters in Table 7. Training is run with DDP on 8 H100 GPUs. The global batch size is 256, and the learning rate is  $3 \times 10^{-5}$ . We train for 3 epochs with cosine annealing and warm up for 10% of total steps. We set the random seed to {42, 43, 44} for Python/NumPy/PyTorch, and enable deterministic behavior where possible.

**Evaluation.** For evaluation, we perform full-pool retrieval over all test items (~134K candidates) for each query item. We compute cosine similarity between the L2-normalized query embedding and each candidate embedding and rank all candidates. We report Hit Rate  $H@K$  for  $K \in \{1, 5, 10, 20, 50, 100\}$ , where a query is considered a hit if any of its positives appears in the top-K ranked list. If a query has multiple positives, we treat it as success when at least one positive is retrieved in top-K.

**Table 7: Training hyperparameters for TGQ-Former.**

Category	Hyperparameter	Value / Setting
General Settings	Framework	PyTorch 2.6.0
	Language	Python 3.10
	GPUs	8×H100 (DDP)
	Precision	fp16
Optimization	Optimizer	AdamW
	Peak learning rate	$3 \times 10^{-5}$
	Weight decay	1e-5
	$\beta_1, \beta_2$	(0.9, 0.999)
	$\epsilon$	1e-8
	Scheduler	Cosine annealing
LoRA Settings	Warm-up ratio	10% of total steps
	Global batch size	256
	$lora_r$	8
	$lora_alpha$	16
TGQ-Former Structure	$lora_dropout$	0
	Target modules	q,k,v,o projections
	Applied layers	all Transformer blocks
	Trainable params	LoRA only (LLM frozen otherwise)
Loss Settings	# random queries ( $T_r$ )	3
	Query dim	768
	Q-Former layers	6
	Conv1D kernel/stride	5/5
TGQ-Former Structure	Dual-gate MLP hidden dim	1024
	Contrastive loss	InfoNCE
	Temperature $\tau$	0.07
	$\lambda_{rr}$ (redundancy reduction)	1
Loss Settings	Embedding normalization	L2-normalize before similarity

## C Lightweight Cropping Preprocessing Baselines

A common heuristic to alleviate border-dominant promotional overlays (e.g., corner badges and banner-like decorations) is to crop the image before feeding it into the vision encoder. In this appendix, we evaluate simple, training-free preprocessing baselines that incur negligible overhead and do not rely on any learned detector.

### C.1 Setup

*Baselines.* We compare three preprocessing variants:

- **No-preprocessing:** the raw image is directly passed to the CLIP image processor.
- **Center-crop (0.9):** center square crop retaining 0.9× the shorter side, followed by the CLIP image processor.
- **Center-crop (0.8):** center square crop retaining 0.8× the shorter side, followed by the CLIP image processor.

*Implementation details.* Given an input image with width  $W$  and height  $H$ , we compute  $S = \min(W, H)$  and crop a centered square region with side length  $s = \lfloor r \cdot S \rfloor$ , where  $r \in \{0.9, 0.8\}$ . The cropped image is then passed through the same CLIP image processor as in the main experiments (including its default resizing/normalization steps). All other components and hyperparameters are kept identical to the main setting.

### C.2 Results

Table 8 reports retrieval performance with lightweight center-cropping. While center-cropping slightly alleviates border-dominant overlays, the improvements remain limited and do not approach those of our method. This suggests that *indiscriminate* suppression of non-product regions is insufficient in practice: useful contextual cues may co-exist with harmful overlay artifacts, calling for

Preprocessing	H@20	H@50	H@100
No-preprocessing	39.60	54.36	65.19
Center-crop (0.9)	39.67	54.44	65.26
Center-crop (0.8)	39.66	54.10	65.22

**Table 8: Lightweight cropping preprocessing baselines. Center-cropping slightly alleviates border-dominant overlays but yields limited gains compared with our method.**

adaptive utilization of auxiliary signals rather than image-only preprocessing.

## D Open-Source Reproducibility on Amazon and Noise Robustness

To mitigate reproducibility concerns under non-releasable proprietary data, we additionally evaluate our method on a public Amazon benchmark. Notably, product images in this benchmark are typically clean and object-centric (often with plain backgrounds), which may under-represent the posterized and noisy conditions observed in real-world e-commerce. We therefore further conduct a controlled robustness study by progressively injecting synthetic visual contamination into images, enabling a matched comparison under increasing noise levels.

### D.1 Dataset: Amazon Clothing, Shoes and Jewelry

We use the *Amazon Clothing, Shoes and Jewelry* subset from the Amazon product metadata corpus (2018 version), and parse the metadata file `meta_Clothing_Shoes_and_Jewelry.json.gz`. Each item is associated with (i) a primary product image URL stored in the `imUrl` field, and (ii) textual metadata including `title`, `brand`, and a hierarchical `categories` field. Following common I2I retrieval setups, we construct positive pairs  $(i, j)$  using dataset-provided related fields, including `also_bought`, `bought_together`, and `also_viewed`. Unless otherwise stated, we treat the related graph as directed and do not symmetrize edges.

*Training set construction.* We first build a valid item pool by scanning `meta_Clothing_Shoes_and_Jewelry.json.gz` and retaining items that satisfy: (i) non-empty `title`; (ii) a non-empty `imUrl`; (iii) a valid category path with at least one category list, where we take the first category path and construct a 3-level hierarchy by truncation, and if its depth is less than 3 we pad by repeating the last level (“relaxed” 3-level parsing); and (iv) the item ASIN is *not* in a pre-generated test ASIN blacklist (constructed below), ensuring train/test separation at the ASIN level.

For each retained item  $i$ , we enumerate its related targets  $j$  from `also_bought`, `bought_together`, and `also_viewed`, and keep a training pair  $(i, j)$  only if  $j$  is also in the valid item pool (and thus also not blacklisted). We then cap the number of training pairs to 1,200,000 by shuffling with a fixed random seed (42) and taking the first 1,200,000 pairs as our training set.

*Test set construction and candidate pool.* We build the test set via pair-based random sampling over the same valid item pool used for training (items with non-empty title, a parsed 3-level category path,

and an accessible image). We first collect all valid ASINs, shuffle them with a fixed random seed (42), and traverse the shuffled list. For each candidate query item  $i$ , we select a single ground-truth neighbor  $j$  by scanning its related field and taking the first valid target that also lies in the valid pool. If such a target exists, we add the pair  $(i, j)$  to the test pairs and include both  $i$  and  $j$  in the test ASIN set. We repeat this process until obtaining 60K test pairs. Items without any valid related target are skipped.

We define the evaluation candidate pool as the set of all unique ASINs appearing in the sampled test pairs (i.e., all query items and their selected targets). For evaluation, each query is associated with a *single* ground-truth target (Top-1) constructed as above, and retrieval ranks all items in the candidate pool. Finally, to avoid ASIN-level overlap between train and test, we export all test ASINs as a blocklist and exclude them from training set construction.

## D.2 Progressive Noise Injection

To emulate real-world e-commerce posterization and background clutter, we generate four image conditions with increasing severity: **(i) Clean**, **(ii) Light**, **(iii) Medium**, and **(iv) Heavy**. For reproducibility, we use a fixed random seed (42) and generate one deterministic corrupted view per test image for each severity level.

*Noise operators.* We consider two synthetic corruption operators:

**Background replacement.** We estimate a foreground mask by thresholding near-white pixels in RGB: a pixel is treated as background if  $\min(R, G, B) \geq 240$ . We keep the complement as foreground and composite it onto a randomly sampled background crop from another image. The background crop is uniformly sampled in location and resized to the original image size; we optionally apply a Gaussian blur with radius  $r_{\text{blur}} = 2$  to the background before compositing.

**Semantic overlay noise.** We add poster-like overlay artifacts that mimic common e-commerce decorations, including (i) *burst badges*, (ii) *corner banners*, and (iii) *top/bottom bars*. For each image, with probability  $p(\text{overlay})$  we sample up to  $N$  overlays uniformly from the three types and render it near the image border. Concretely, the overlay anchor is sampled from one of the four corners with a 10% margin: the top-left/top-right/bottom-left/bottom-right region, where the  $(x, y)$  position is uniformly sampled within the corresponding margin box. The overlay geometry is scaled relative to image size: burst badges use a star-shaped polygon with radius in  $[0.15, 0.20] \cdot \min(W, H)$ ; corner banners are filled triangular patches with side length in  $[0.35, 0.45] \cdot \min(W, H)$  (top-left or top-right); and bars are rectangles with height in  $[0.15, 0.20] \cdot H$  placed at the top or bottom. We render short marketing text in white on top of the overlay using a fixed font (Arial when available, otherwise a default font), with text sampled from small, fixed vocabularies (e.g., badge: {HOT, SALE, 50%, NEW, No. 1, TOP, 9. 9, Best}; banner/bar: {Free Shipping, Flash Sale, New Arrival, Limited Offer}).

*Severity levels.* We instantiate four severities by controlling the application probability and intensity of the above operators (Table 9). When both operators are enabled, we apply background replacement first and then overlay noise.

**Table 9: Noise hyperparameters for the progressive robustness test.**

Severity	$p(\text{bg repl.})$	$p(\text{overlay})$	#overlays
Clean	0.0	0.0	0
Light	0.0	0.4	1
Medium	0.5	0.7	3
Heavy	0.8	0.9	5

**Table 10: I2I retrieval on Amazon Clothing, Shoes and Jewelry under progressive noise.**

Setting	Method	H@10	H@20	H@50
Clean	NoteLLM-2	46.05	57.12	69.41
	Ours	46.02	57.18	69.46
Light	NoteLLM-2	45.79	56.76	68.93
	Ours	45.92	57.03	69.27
Medium	NoteLLM-2	45.01	56.05	68.11
	Ours	45.33	56.48	68.73
Heavy	NoteLLM-2	44.28	55.37	67.55
	Ours	44.91	56.04	68.33

## D.3 Compared Methods and Evaluation Protocol

We compare our method with the strongest connector-based baseline: **NoteLLM-2** [34]. All methods share the same vision encoder and LLM embedding backbone as in the main experiments unless otherwise stated. We follow the standard top- $K$  retrieval evaluation and report Hit Rate@ $K$  (H@ $K$ ) for  $K \in \{10, 20, 50\}$ . For each test query, candidates are all items in the candidate pool (all unique ASINs in the sampled test pairs), and the ground-truth neighbor is the paired target in the test pairs.

## D.4 Results: Accuracy under Increasing Noise

Table 10 reports retrieval accuracy on Amazon under progressive noise. We highlight two aspects: (i) **clean-setting performance**, which reflects transferability to object-centric images; (ii) **degradation curves** as noise increases, which measures robustness to posterization-like corruptions. We expect both methods to perform similarly on Clean images, while our method should degrade more gracefully under Medium/Heavy noise due to its reliability-aware visual extraction and calibration.

*Discussion.* On the clean benchmark, both approaches operate on high-quality object-centric images, and the gap can be small. As we increase the noise severity, the baseline can be distracted by high-contrast overlays and altered backgrounds, leading to larger performance drops. In contrast, our method is designed to selectively trust visual evidence conditioned on its reliability, and thus should maintain more stable retrieval quality under Medium/Heavy noise.